Mon. Not. R. Astron. Soc. **000**, 1–15 (2015) Printed 12 January 2015 (MN LATEX style file v2.2)

Benchmarking the power of amateur observatories for the TTV exoplanets detection. TTV and RV data releases for ten planet-hosting stars.

Roman V. Baluev[1,2]*, Evgenii N. Sokov[1], Vakhit Sh. Shaidulin[2,1], Iraida A. Sokova[1], Hugh R. A. Jones[3], Mikko Tuomi[3,4], Guillem Anglada-Escudé[3,5], Paul Benni[6], Carlos A. Colazo[7], Matias E. Schneiter[8], Carolina S. Villarreal D'Angelo[8], Artem Burdanov[9], Eduardo Fernández-Lajús[10,11]

[1] *Central Astronomical Observatory at Pulkovo of Russian Academy of Sciences, Pulkovskoje shosse 65, St Petersburg 196140, Russia*
[2] *Sobolev Astronomical Institute, St Petersburg State University, Universitetskij prospekt 28, Petrodvorets, St Petersburg 198504, Russia*
[3] *University of Hertfordshire, Centre for Astrophysics Research, Science and Technology Research Institute, College Lane, Hatfield AL10 9AB, UK*
[4] *University of Turku, Tuorla Observatory, Department of Physics and Astronomy, Väisäläntie 20, FI-21500, Piikkiö, Finland*
[5] *School of Physics and Astronomy, Queen Mary University of London, 327 Mile End Road, London E1 4NS, UK*
[6] *Acton Sky Portal (Private Observatory), Acton, MA, USA*
[7] *Observatorio Astronómico, Universidad Nacional de Córdoba, Laprida 854, Córdoba X5000BGR, Argentina*
[8] *Instituto de Astronomía Teoríca y Experimental, Universidad Nacional de Córdoba, Laprida 854, Córdoba X5000BGR, Argentina*
[9] *Kourovka Astronomical Observatory of Ural Federal University, Mira str. 19, Ekaterinburg 620002, Russia*
[10] *Universidad Nacional de La Plata, Paseo del Bosque S/N, 1900 La Plata, Argentina*
[11] *Instituto de Astrofísica de La Plata, Observatorio Astronómico, Argentina*

in original form 2015 January 26

ABSTRACT

We perform an analysis of more than 80000 photometric measurements for the following 10 stars hosting transiting planets: WASP-2, -4, -5, -52, Kelt-1, CoRoT-2, XO-2, TrES-1, HD 189733, GJ 436. The analysis includes mainly the photometric data from the Exoplanet Transit Database, public data from the literature, and some proprietary data privately supplied by other authors. We present ~ 300 transit timing measurements derived from these data, as well as improved planetary transit parameters.

Additionally, for 5 of these 10 stars we present a set of radial velocity measurements obtained from the spectra stored in the HARPS and HARPS-N archives using the HARPS–TERRA pipeline.

Our analysis of these TTV and RV data did not reveal significant hints of additional orbiting bodies in almost all of the cases. In the WASP-4 case, we found hints of marginally significant TTV signals having amplitude $10 - 20$ sec, although their parameters are model-dependent and uncertain, while radial velocities did not reveal statistically significant Doppler signals.

Key words: methods: data analysis - methods: statistical

1 INTRODUCTION

The first extrasolar planet, orbiting a solar-type star 51 Pegasi, was discovered by Mayor & Queloz (1995), based on the precision Doppler measurements of the ELODIE spectrograph. After that, the number of the detected exoplanets grew continuously, exceeding 1000 so far. In fact, 20 years ago a new rapidly-growing domain of fundamental science was created, devoted to the exoplanets research.

Currently, most of the known exoplanetary candidates were detected by one of two major techniques: the radial velocity (RV) method or transit method that increased its output in recent time thanks to the launch of specialized spacecrafts CoRoT (ESA) and Kepler (NASA).

Unfortunately, both the Doppler and transit exoplanet detection methods require sophisticated and expensive instrumentation and remain practically inaccessible to the ma-

* E-mail: r.baluev@spbu.ru

© 2015 RAS

jority of the community. The RV method requires the use of extremely stable spectrographs. There is only about a dozen of such spectral instruments in the world that are capable of detecting an exoplanet. The transit detection is also difficult. It requires a very lucky orientation of the planetary orbit, whereas the transit event is rather short in time, although periodic. To detect a transiting planet, we have to observe lots of stars, and necessarily this would be largerly a naught work. This requires the use of specialized ground-based robotic telescopes or telescope networks, or space observatories like the above-mentioned CoRoT and Kepler. Organizing any of such a campaign is a difficult task even for professional scientific teams.

In terms of the photometric accuracy and quality, ground based telescopes are no match to spacecrafts like Kepler. But all space projects have a common disadvantage: they are severely limited in time, while the sensitivity to weak planetary signals in the data degrades quickly when the planetary orbital period exceeds the observations time base. This means that Kepler data cannot reliably detect long-period planets, analogous to the giant planets of Solar System. In any course of actions, the responsibility of follow-up tracking always returns to ground-based observatories. Ground-based observations of planetary transits are much less demanding than precision radial velocity measurements, and of course much cheaper than projects like Kepler. In fact, such observations are pretty possible even with the amateur equipment. Thus, the exoplanetary hunt can potentially become a "citizen science" that can trigger a qualitative leap in the field.

However, amateur observatories, even when organized in a network, are unable to undertake efficient transit surveys like e.g. SuperWASP or others. It is necessary to use the observation time more efficiently than in a classic transit survey. This goal can be achieved by means of the transit timing variation (TTV) method. In this approach, we may deal with a list of well defined targets that are continuously monitored. Each target is a known host of a transiting planet, and its transits are regularly observed. If more planets orbit the host, they should induce perturbational effects on the motion of the transiter, causing observable delays to its transits, in comparison with a strictly periodic ephemeris. The TTV method allows to spend the observation time more efficiently, because we know what targets should be observed, and when.

This work represents an attempt to determine the practical efficiency of such an approach, based on the photometry data, taken mainly from the Exoplanet Transit Database (ETD) of the Chech Astronomical Union, `http://var2.astro.cz/ETD/`.

Currently, about 30 amateur and professional observatories are regularly contributing to the database. This network offers telescopes of different apertures – from 20 cm to 2.6 m, – and located in Russia, NIS countries, and many other places of the world: Europe (7 EU countries), Americas (Argentina, USA, Canada), Australia, Oceania (Cook isles). The locations are labelled in the map of Fig. 1. The observational programme involves currently ~ 20 transiter hosts that are more or less regularly observed. For some of the stars, several years of observations are already available. However, the transit fitting algorithm used by ETD is quite simplified and imperfect, and this was already noted by other authors. In this work we present a new data reduction pipeline that handles subtle photometric effects (like the red noise) more accurately. This pipeline was developed to deal with the photometry of a relatively poor or moderate quality, which is typical for the amateur data in ETD.

Table 1. Sources of the photometric data (except for ETD).

target	references
HD 189733	Bakos et al. 2006; Winn et al. 2007a; Pont et al. 2007
TrES-1	Winn et al. 2007b
XO-2	Fernandez et al. 2009
GJ 436	Bean et al. 2008; Shporer et al. 2009; Stevenson et al. 2012
CoRoT-2	Gillon et al. 2010
Kelt-1	Siverd et al. 2012
WASP-2	Southworth et al. 2010
WASP-4	Wilson et al. 2008; Gillon et al. 2009; Winn et al. 2009; Southworth et al. 2009b; Sanchis-Ojeda et al. 2011; Nikolov et al. 2012; Petrucci et al. 2013
WASP-5	Southworth et al. 2009a

We do not limit ourselves to only amateur observations or only ETD. We also use photometric data published in the literature. Moreover, for our targets we revealed a moderate amount of the spectra stored in the HARPS and HARPS-N archives, and we derive RV data from them to provide and independent "calibration" of our TTV results. However, in this work we have no goal to perform a fully self consistent TTV+RV analysis. Instead, we aim to characterize the accuracy and reliability of the TTV data that we can derive from just the photometry.

The structure of the paper is as follows. In Sect. 2 we provide a detailed description of all the data that we include in our analysis. In Sect. 3 we introduce the algorithms used to process the photometric data. In Sect. 4 we present the TTV data derived from the photometry and describe the results of their periodogram analysis. In Sect. 5 we give the remaining fitted parameters of the planets considered in the work. In Sect. 6 we describe the RV data obtained for some of our targets on the base of the spectra found in the HARPS/HARPS-N archives. In Sect. 7 we discuss in details the case of WASP-4, for which we detected possible hints of a weak TTV signal.

2 THE SOURCE DATA

Our primary source of the photometric data is the Exoplanet Transit Database (ETD). We extracted a set of the best transit lightcurves from ETD for 10 selected stars. Also, we added in our analysis several public transit lightcurves that we found in the literature. Thus, our photometric data cover 10 targets with about 300 transit lightcurves, and about 80000 individual photometric measurements. The public data were presented in the works listed in Table 1, and most are stored in the Vizier database. We obtained approximately half-and-half splitting between the ETD and non-ETD data (in terms of the number of potometric measurements).

We need to note that the data from (Sanchis-Ojeda

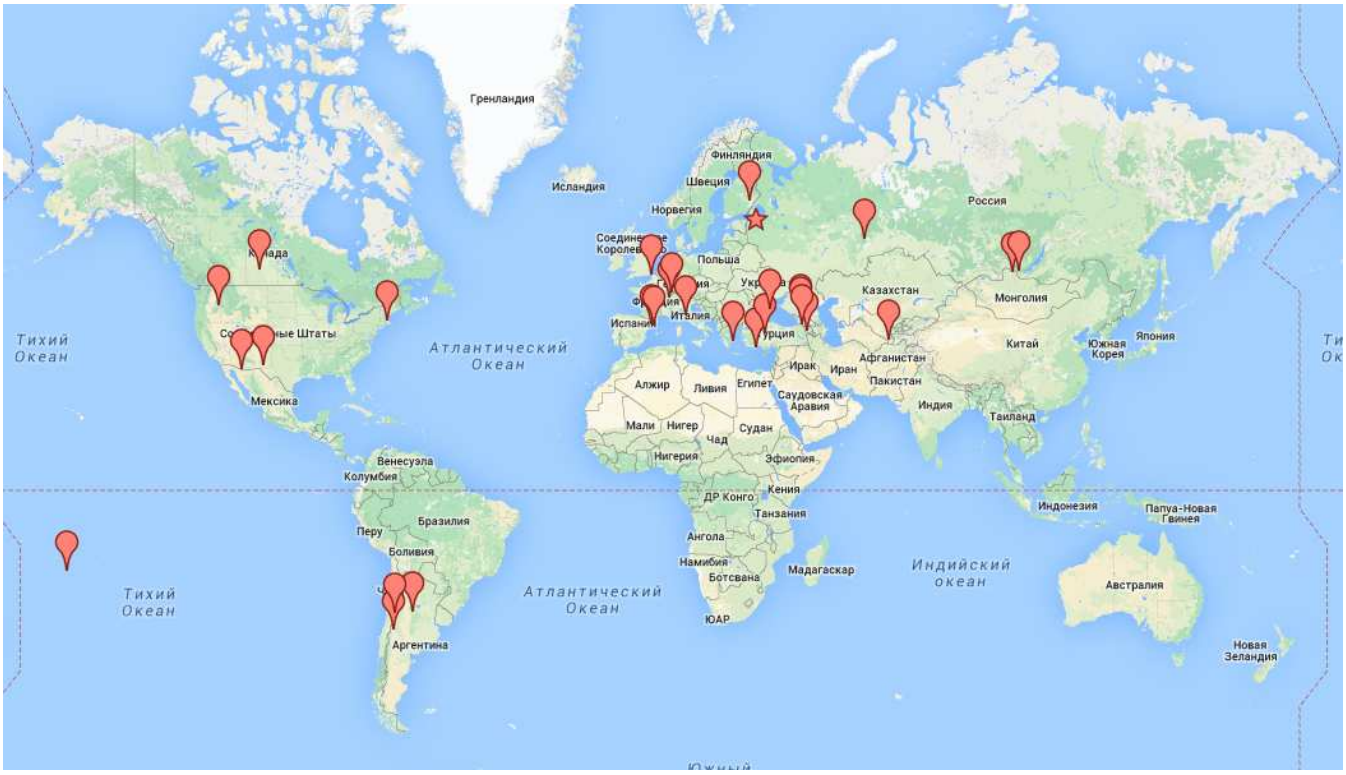


Figure 1. World distribution of the observatories contributing to the ETD database.

et al. 2011) also contain reprocessed photometry from (Winn et al. 2009), so the original Winn et al. (2009) data were not actually included in our analysis. Also, we eventually decided to drop off the HST data by Bean et al. (2008), because they all appeared to cover only small parts of a transit and could not produce good precision in the derived mid-times. The photometry presented by Petrucci et al. (2013) is not public, but it was kindly released to us by the authors. The data from (Southworth et al. 2009a,b, 2010) appeared not very reliable due to the telescope clock errors, but their photometry is rather accurate in itself, and thus they are still useful in constraining all transit parameters except for mid-times (e.g. by adding a fittable time offset to these light curves model relatively to the other lightcurves). All timings in the photometric data were transformed to the $\mathrm{BJD_{TDB}}$ time stamps by means of the public IDL software developed by Eastman et al. (2010).

Additionally, we used the precision radial velocity (RV) obtained from the spectra of the HARPS archive, available for the following targets from our photometry sample: WASP-2, -4, -5, HD 189733, Corot-2. These spectra were processed with the advanced HARPS–TERRA pipeline that offers an improved RV accuracy (Anglada-Escudé & Butler 2012). The number and quality of these RV data is usually not very high, because many of these targets are rather faint for HARPS.

For GJ 436 we found a large amount of high-quality HARPS RV data, as well as a large Keck RV time series recently published by Knutson et al. (2014). However, it appeared that this case deserves to be investigated detailedly in a separate work, so in this paper we only present our TTV data for GJ436, derived in the common way as for the other stars.

In this work we do not perform the joint transits+RV fits, because it appeared that to perform such an analysis at a desirable level of quality, we must provide a solution to several non-trivial issues that fall outside the scope of this paper. These issues include, e.g., the treatment of the correlational structure of the RV noise, and treatment of the RV points affected by the Rositter-McLaughlin effect. In this work we used the RV data mainly as an independent source of adjudgement information.

3 METHODS OF THE TRANSIT LIGHTCURVES ANALYSIS

3.1 Details of the transit model and its parametrization

Let us first adopt the approximation that the transiting planet moves along a straight line with constant velocity, thus neglecting the orbital curvature of its actual trajectory during the transit. The model of the linear motion allows to easily predict the separation between the centers of planet and star disks, δ, as a function of the time. We have 4 kinematic characteristics of the transit that must be fitted: (i) the mid-time of the transit t_c, (ii) the duration of the transit t_d, defined as the time spent between the first and fourth contacts, (iii) the projected planet radius r, and (iv) the impact parameter b, measuring the smallest projected separation δ. Given these parameters and easy geometric constructions, the projected separation δ can be expressed as:

$$\delta(t) = \sqrt{b^2 + [(1+r)^2 - b^2]\,\tau^2}, \quad \tau = 2\frac{t-t_c}{t_d}, \quad |b| \leqslant 1+r. \quad (1)$$

This assumes that the star radius is unit. To simplify the formula for δ and simultaneously get rid of the non-trivial definition domain for b, our algorithm adopts internally a replacement of the impact parameter b:

$$b = \frac{p}{\sqrt{1+p^2}}(1+r). \quad (2)$$

With the new parameter p we do not need to take care of its definition domain: any real value of p is physically meaningful. Thus we eliminate the danger that this parameter can walk to a forbidden domain during the fit. With p replacing b, we have

$$\delta(t) = (1+r)\sqrt{\frac{\tau^2+p^2}{1+p^2}}. \quad (3)$$

However, this approximation of $\delta(t)$ might be inaccurate due to the curvature of the planet trajectory. In this work we include a correction to this formulae, assuming that the planet moves along a circular orbit. In this approximation, the projected distance can be expressed by the same formulae (1) and (3), substituting the following quantity τ' instead of τ:

$$\tau' = \frac{\sin\tau\alpha}{\sin\alpha}, \qquad \alpha = \pi\frac{t_d}{P} \ll 1, \quad (4)$$

where P is the transiter's orbital period. The auxiliary angle α reflects the curvature of the circular orbit.

The trajectory curvature also depends on the orbital eccentricity, but usually this eccentricity is difficult to determine from transit observations reliably, and we have no other option except to assume that it is zero. A zero eccentricity is a good prior assumption for the most of these short-period planets. In the cases when radial velocity data are also available, the accurate eccentricity information can be obtained from the joint transit+RV fits, but we do not perform fits of such type in this work.

After the function $\delta(t)$ is calculated, we approximate the relative flux reduction with the use of the stellar limb darkening model by Abubekerov & Gostev (2013). These authors provided theoretic formulae for various types of the limb darkening effect, as well as a software library written in C. The library provides subroutines to compute the observed light flux reduction ΔL as a function of the eclipsing planet radius r and of the projected separation δ (assuming that the star radius is unit), as well as of the limb darkening coefficients that depend on the selected model. Besides, this library provides partial derivatives of ΔL with regard to its arguments. These derivatives are necessary to compute the gradient of the likelihood function, which is also used by the transit fitter.

Thus for a transit lightcurve we have 4 fittable parameters of the planet or planetary orbit: the planet/star radii ratio r, the transit mid-time t_c, the transit duration t_d, and the impact parameter replacer p. As the orbital period P is known for all our planets with a very good accuracy, we treat it as a fixed parameter in the formula (4).

Additionally, there are two parameters determining the limb darkening model. In this work we use a quadratic two-term model of the stellar limb darkening with two coefficients to be determined, A and B. The brightness of a point on the visible stellar disc, observed at a given separation from its center, ρ, is modelled as

$$\begin{aligned} I(\rho) &= 1 - A(1-\mu) - B(1-\mu)^2 = \\ &= 1 - A - 2B + (A+2B)\mu + B\rho^2, \\ &\quad \mu = \sqrt{1-\rho^2}. \end{aligned} \quad (5)$$

However, in practice the brightness model (5) can easily turn non-physical, if the coefficients A and B are allowed to attain arbitrary values. This becomes a significant problem if our data are polluted by some systematic errors that are always difficult to foresee in advance. There are a couple of natural basic constraints that we place on the coefficients A and B to keep the model (5) physically reasonable:

$$I(\rho) \geqslant 0, \quad \frac{dI}{d\rho} = [2B\mu - (A+2B)]\,\frac{\rho}{\mu} \leqslant 0, \qquad \forall\rho \in [0,1]. \quad (6)$$

If the second condition (the one on the derivative) is satisfied, $I(\rho)$ is a monotonic non-increasing function, so the condition $I(\rho) \geqslant 0$ for $\rho \in [0,1]$ is then equivalent to $I(1) = 1 - A - B \geqslant 0$. In the second condition, the expression in parenthesis is a linear function of μ, so to have it always non-positive for $\mu \in [0,1]$, it is necessary and sufficient to have it non-positive at the boundaries $\mu = 0$ (disk limb) and $\mu = 1$ (disk center). Finally, we have total of three elementary inequality constraints on A and B to satisfy:

$$A + B \leqslant 1, \quad A + 2B \geqslant 0, \quad A \geqslant 0. \quad (7)$$

Note that the coefficient B is allowed to be negative here (but $B \geqslant -1$). We do not put an extra condition $B \geqslant 0$. Negative values of B mean that the limb-darkening gradient is diminishing (in absolute value) closer to the limb, although it never turns positive (any "limb brightening" is disallowed).

We may satisfy (7) by means of making a smooth replace of the parameters A and B, such that the formulae of the replace would disallow the conditions (7) to be broken. This can be reached, for example, by the following trigonometric replace:

$$A = \sin^2\theta\,(1-\cos\varphi), \quad B = \sin^2\theta\cos\varphi. \quad (8)$$

Obviously, whatever real values the new auxiliary parameters θ and φ might attain, the resulting values of A and B always satisfy (7). From the other side, each point (A,B) in the domain (7) maps to some pair (θ,φ) with real values of the parameters:

$$\sin^2\theta = A + B, \quad \cos\varphi = \frac{B}{A+B}. \quad (9)$$

Note that from (7) it follows that $A + B \geqslant |B|$, meaning that $A + B$ is never negative.

Therefore, treating the auxiliary angles θ and φ as primary fittable parameters, we can satisfy the conditions (7) automatically. The result of the fitting would correspond to either an internal point of the domain (7), or to some point on its boundary, if the actual data suggest to move the solution to a non-physical domain due to e.g. their poor statistical quality or systematic errors. The boundary points correspond to certain special values of θ and φ that can be easily identified: $\theta = \pm\pi/2 + \pi k$ on the first boundary of (7), $\varphi = \pi + 2\pi k$ on the second boundary, and $\varphi = 2\pi k$ at the third boundary.

3.2 Details of the fitting procedure

In our analysis we focus on obtaining the TTV deviations with maximum accuracy achievable with these photometric data. Because the ETD data, even after the pre-selection, often have only a moderate quality, performing a complete and independent fit per each transit lightcurve is not a good option. The accuracy of thus obtained transit parameters would often be pretty bad, and this would impact the accuracy of the fitted TTV data as well. Moreover, the transit fits for individual lightcurves sometimes do not even converge to a reasonable result due to e.g. incomplete coverage of the transit or presence of significant curved trends.

To overcome these issues, we adopt in this work the following approach. We perform a *joint* fit of all transit lightcurves, available for a given star, assuming that most of the transit parameters, except for the mid-times, are equal for different lightcurves. Such a "shared" transit parameter is still fittable, taking into account the constraint of its values being equal between different lightcurves. The mid-times are fitted individually for each lightcurve, i.e. they remain unconstrained.

Such an approach allows to use the full statistical power of all photometric data, available for a given star, to fit the shape of the transit curve, but still fitting the TTV offsets of individual transits separately from each other. We can note the following potential weaknesses of this approach:

(i) It is not taken into account that the limb darkening coefficients depend on the photometry band, which are different for different lightcurves. Therefore, the results of such fitting method would refer to some averaged limb darkening, possibly introducing minor modelling errors in individual lightcurves. From the other side, the limb darkening effect in the transit curve is always symmetric relatively to the mid-time, implying that its impact on the derived mid-times should be small, if not negligible. In fact, we noticed that even fitting of a transit model without any limb darkening at all does not change the derived TTV data significantly (beyond the estimated parametric uncertainties). However, in the final version of our algorithm we decided to disentangle the limb darkening coefficients for the best lightcurves (those that have r.m.s. smaller than 10 per cent of the transit depth) and fit these coefficients independently.

(ii) It is not taken into account that transit duration may also be subject to variations, like the transit mid-time. However, in practice it appeared that the accuracy of the transit duration estimations by roughly an order of magnitude worse than those of the mid-times. Moreover, some lightcurves cover the transit event only partially, implying that its duration would remain almost unconstrained when fitted anew. Besides, the potential magnitude of perturbations, generated by an unseen planet in the transit duration is usually smaller than in the transit mid-times. The reason is that the mid-time is basically tied to the orbital phase of the transiter, while the transit duration is related to the changes of its orbital semimajor axis (if the eccentricity is negligible). The perturbations may have a cumulative effect in the orbital longitude, making them more sensitive, while the semimajor axis is a rather resistent and long-term stable dynamical quantity, and the eccentricity is close to zero in the most cases of transiting planets. Therefore, we believe it is pretty safe to neglect the possible transit duration variations in this work. At least, any perturbations from an unseen planet should be better detectable in the simultaneously more accurate and more sensitive TTV data, and only after that it might be reasonable to consider TDV.

(iii) The mid-times estimations, obtained in such a manner, are not necessarily mutually uncorrelated. These mid-times are correlated with the remaining transit parameters, which are now shared between the lightcurves. Through this effect, some cross-correlation between the estimated mid-times may appear. This creates a risk of additional statistical effects in the derived TTV data, like e.g. the non-white noise. However, the magnitude of these TTV correlations usually remains very small (maximum of $1-3$ per cent, and ~ 0.1 per cent in average), and no deviations from the white noise are seen in the periodograms of the TTV data. More significant (> 10 per cent) TTV correlations can appear for lightcurves that offer only a partial coverage of the transit, but such lightcurves represent only a minor fraction of our data.

In addition to the planetary transit itself, our lightcurve models include a polynomial trend with fittable coefficients. Such a trend is necessary to take into account various drifting effects, e.g. the effect of airmass or other types of systematic variations that appear frequently in our data. Each transit lightcurve has an individual fittable trend with an separate set of trend coefficients. After some experimenting with the data, we found that cubic trends represent a good compromise between the model adequacy and its parametric complexity. We did not try to reduce this systematic photometric variation based on its correlation with the airmass function: while for some lightcurves such a correlation looked clear, for others it was not obvious, indicating that other systematic effects were in the game.

The lightcurves model is relatively complicated, while the photometry used in this work is not of a very good quality. In practice we often faced difficulties causing the fitter to be trapped in the local maxima of the likelihood function, which was related to an unrealistic branch of the solutions. For example, without a special care we frequently obtained non-physical solutions corresponding to a grazing transit with $r \gg 1$. Also, some lightcurves do not cover the complete transit, and in such cases the fitting of the transit mid-time is complicated by its strong correlation with the coefficients of the polynomial trend. To avoid such traps, we worked out the following sequence of auxiliary preliminary fits:

(i) Perform a preliminary fit constraining the mid-times at a regular grid (with free scale and offset), implying all TTV residuals are zero by definition; fixing the impact parameter p at an intermediary value of 1 ($b \approx 1/\sqrt{2}$), and fixing the limb darkening coefficients at $A = B = 0.25$ (or $\theta = \pi/4$ and $\varphi = \pi/3$).

(ii) Refit after releasing the mid-times and impact parameter, but still holding the limb darkening coefficients fixed.

(iii) Refit after releasing the limb darkening coefficients (binding them across different lightcurves).

(iv) Refit after full release of the limb darkening coefficients for the best lightcurves (those with r.m.s. < 0.1 of the transit depth).

After that, we also apply the red-noise detection and fitting procedure as described in the section below.

3.3 Reduction of the red noise

It is already known well that stellar photometric data usually include a correlated ("red") noise component that has an important effect the fitted transit parameters (Pont et al. 2006; Winn et al. 2008; Carter & Winn 2009). An easy technique to calculate the effect of the red noise on the fitting uncertainties was introduced in these works. Although these authors avoid making restrictive assumptions concerning the correlation structure of the red noise, their method still remains rather simplistic and it does not allow to take into account, for instance, the systematic bias in the fitted parameters. Additionally, these methods may rely on the out-transit photometric data, which are very limited in our case.

In this work we apply the approach based on a parametric modelling of the noise covariance matrix. This is an adaptation of the red-noise fitting technique from (Baluev 2011, 2013b, 2015) that was developed to handle exoplanetary radial-velocity data, in which the noise correlations may appear e.g. due to the stellar activity. In this approach we approximate the red noise by a stationary Gaussian random process with a covariance function of a given functional form. The covariance coefficient between two arbitrary photometric observations x_i and x_j, acquired at the times t_i and t_j, is modelled as

$$V_{ij} = \mathrm{Cov}(x_i, x_j) = \sigma^2_{i,\mathrm{wht}}(p_{\mathrm{wht}})\delta_{ij} + V_{ij,\mathrm{red}}(p_{\mathrm{red}}, \tau),$$
$$V_{ij,\mathrm{red}} = p_{\mathrm{red}} R_{ij}(\tau), \quad R_{ij} = \rho\left(\frac{t_i - t_j}{\tau}\right), \qquad (10)$$

with p_{wht}, p_{red}, and τ being free fittable parameters. Here, the first noise term, $\sigma^2_{i,\mathrm{wht}}$, represents the white fraction of the noise, detailed below. The red noise is given by the second term, V_{ij}, which also depends on the function $\rho(t)$ that represents an adopted shape of the correlation function. We use mainly the exponential correlation function $\rho(t) = \exp(-|t|)$. This definitely not a unique choice, but in practice this model of the red noise usually appears pretty enough.

The white-noise term $\sigma^2_{i,\mathrm{wht}}$ in (10) is a matter of a separate discussion. We believe that physically the so-called additive model would be more suitable here. In this model, the value $\sigma^2_{i,\mathrm{wht}}$ is determined as a sum of the stated instrumental variance and of an unknown fittable "jitter" variance, generated by e.g. Earth atmospheric instability, or by unassessed instrumental instability, or by short-term (minutes to hours) intrinsic variations of the stellar flux, whenever these variations can be treated as a white noise. Although, we must note that in practice the instrumental uncertainties in our data do not look very trustable, and often they are just omitted, forcing us to assume that the measurements have just equal uncertainties. Therefore, in any case we should not expect that our white noise can be accurately modelled from the physical point of view. In these circumstances, the noise model should be chosen mainly on the basis of mathematical simplicity or usefullness, relying on only minimal or no knowledge of the underlying physics. Given all this in mind, we eventually decided to use in our work a regularized noise model defined in (Baluev 2015). In the majority of practical cases, this model should be just equivalent to the additive noise model, possessing more smooth mathematical behaviour otherwise. This regularized model proved rather resistant with respect to various pitfalls appearing during the fitting procedure.

The fitting of the compound model, involving simultaneously the models of the transit curve and of the photometric noise, is done by means of the maximum-likelihood approach with details given in (Baluev 2015). That work was devoted primarily to the analysis of the radial velocity data, but mathematically the methods that we are using here are identical.

However, after an attempt to apply this technique in practice we faced a difficulty appearing because far not all lightcurve data in our set demonstrated a well fittable red noise. In fact, only 1/3 to 1/2 of the lightcurves allowed to perform such a fitting reliably, while in the other cases the red noise was either not detectable, or its magnitude estimation became pretty small (in comparison with its determination uncertainty). Such cases lead to model degeneracies and decrease the reliability of the entire fit for a given star. Thus, we added to our analysis pipeline a set of auxiliary fits in order to identify the lightcurves, in which the red noise could be modelled more or less reliably. Namely, we tried to perform a series of probe fits, adding a red noise term to the model of each transit lightcurve subsequently. If the red noise could not be estimated reliably, more accurately if the relative uncertainty of its estimated mangitude exceeded 2/3, the relevant red noise term was removed from the model and this lightcurve was further treated as having purely white noise. Otherwise, we proceeded to the next probe fit preserving this red noise term in the model. In the end, after all individual lightcurves were processed in such a way, we performed one more check of each red noise term (because some of these terms could turn insignificant after the other terms being added) and the final fine fit.

The quality of such an approach of the red noise reduction is examined in Fig. 2. The best way to observe a "non-white" noise is to look at its power spectrum: the white noise should have constant power in average, while the red noise should demonstrate a systematic uprise to long periods. In our case we compute the so-called residual periodograms (see Baluev 2015) for each individual lightcurve, and then compute their average per each star involved in the analysis. These averaged periodograms is what is plotted in Fig. 2. For each star, we use subsequently three base photometric models: (i) just transits witout any limb darkening plus the white noise; (ii) same as model (ii) plus cubic trends and taking into account the effect of the quadratic limb darkening; (iii) same as model (ii) plus the red noise term.

We can clearly see from Fig. 2 that the long term photometric variations are not reduced to just trends. Although the trends themselves are also important, after their removal the power spectra still contain an additional power in the frequency range of > 10 min^{-1}. The trends can only affect the frequency domain of $> 200-300$ min^{-1} (this corresponds to the typical time span of the lightcurves). In the most cases, our red-noise model allows to remarkably suppress the remaining excessive power, at least by the factor of 2. We must acknowledge that the reduction of this red noise looks rather difficult and still is incomplete.

Some statistical information on the derived red noise

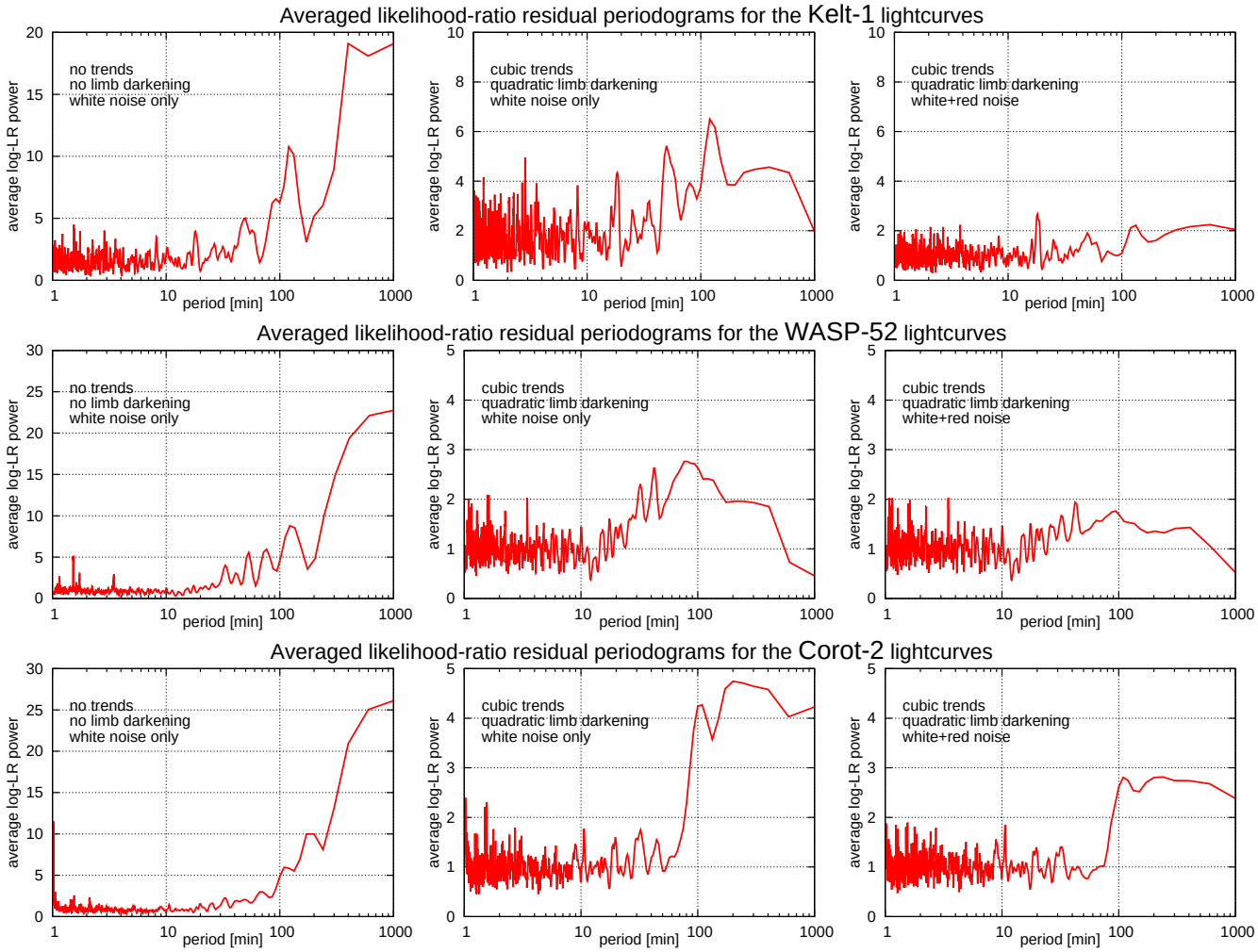


Figure 2. Examining the effect of the red noise in the lightcurve photometry for a few of stars belonging to our sample. Please note that plots in the first column have different ordinate scale than those in the other two. See text for the detailed discussion and explanation.

characteristics now follows. About 60 per cent of lightcurves did not contain any detectable red noise at all. For the remaining 40 per cent of lightcurves, the red noise caused an increase of the TTV uncertainty by a factor of 1.3 in average (a median value). This is not very large, although a minor fraction of the mid-times demonstrated a more remarkable increase of the uncertainty, up to by a factor of $2-3$. Concerning the derived mid-times themselves, the average TTV bias due to the red noise was only about 1/6 fraction of the uncertainty, and only a few points demonstrated a shift above 1σ.

Summarizing, in the majority of the cases, either there was no any detectable red noise, or the change in the TTV data was small, even if the red noise term was detectable. Nonetheless, it is important that some individual TTV points are affected much more.

3.4 Testing the Gaussianity of the noise and clearing away the outliers

In the data-analysis methods described above, we largely relied on the assumption that the photometric noise is Gaussian. This assumption needs some verification, which we performed in the following manner. After fitting of all the data, we computed the residuals and normalized them by their relevant modelled uncertainty (square root of the sum of the estimated white and red noise variances). If the noise was Gaussian, the distribution of these normalized residuals should be close to the standard Gaussian, and vice versa. We consider the entire set of $\sim$ 80000 normalized residuals for all stars involved in our analysis, and plot the relevant distribution in Fig. 3

As we can see, the empiric distribution is indeed almost Gaussian, except for the very tails ($>$ 4-sigma deviation). The empiric distribution has heavier tails. However, by removing of several points in the distribution tails we can reach very good agreement with the Gaussian approximation. In fact, these 11 points represent outliers and should be removed in any case. The final results below correspond to the data with these outliers removed.

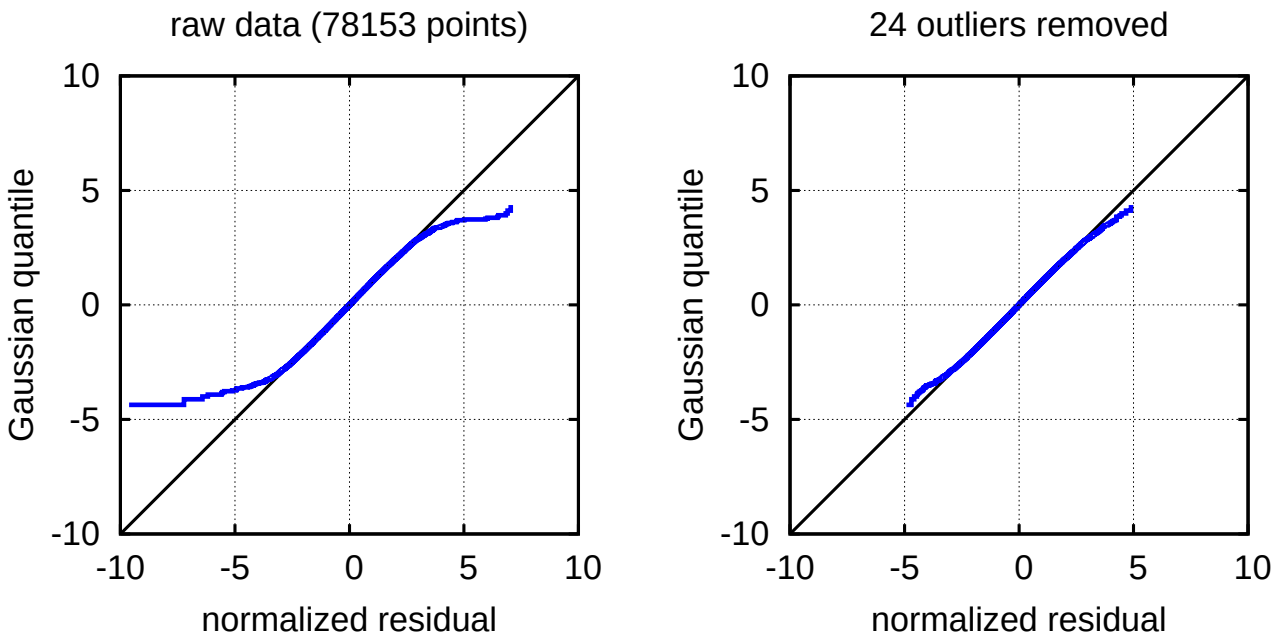


Figure 3. Testing the normality of the entire ~ 80000 photometric data used in the work. Abscissa shows the value of the best fitting residual, normalized by its total modelled variance (for white+red noise). The ordinate contains the normal quantiles of the empirical cumulative distribution of these normalized residuals. Perfectly Gaussian residuals should all lie close to the main diagonal that represents a standard normal distribution, while a deviation from the diagonal indicates a non-Gaussian noise.

4 DERIVED TTV DATA AND THEIR ANALYSIS

Using the fitting techniqe described above, we computed the mid-times for each observed transit, and now release these TTV measurements and other accompanying data in the online supplement to the article. The supplement represents a file containing a text table. The meaning of the columns in this file is described in Table 2. This file only contains the parameters that are attached to individual lightcurves. The common fit parameters that are shared between different lightcurves are given separately in Sect. 5 below.

The TTV residuals for these data are plotted in Fig. 4. In Fig. 5 we verify the normality of the distribution of the TTV noise present in these derived data in the way similar to Sect. 3.4. In the TTV residuals we find no obvious outliers or deviations from the Gaussian distribution. The apparent excess in the distribution tails that can be seen in the left panel of Fig. 5 is uncertain due to a relatively small number of the TTV data. Nonetheless, we identified 9 possible "candidate outliers", and tried to remove them together with 7 TTV points referring to the Southworth et al. (2009a,b, 2010) data. The TTV analysis discussed below was performed for the full TTV data set as well as for the reduced one.

First, we made an effort to detect possible long-term curvatures in our TTV. This was done by means of modelling the mid-times by a quadratic function (instead of only linear that would correspond to strictly periodic transits). None of the TTV time series demonstrated a long-term quadratic variation with at least 2-sigma significance (the most suspicious cases had 1.5σ to 1.7σ).

Second, we undertook a periodorgam analysis of the TTV residuals, in order to reveal possible periodic perturbations from any additional unknown planets orbiting these stars. We again applied "residual periodograms" similar to the ones that were used to plot Fig. 2 above. Now our null model included a quadratic trend that is related to the period of the main (transiting) planet and a white noise with a fittable additive "jitter". The alternative model also included a sinusoidal signal at a probe frequency. None of these periodograms demonstrated any signs of a non-white noise, and in fact almost all appeared consistent with the pure noise model, although the cases revealing significant excessive TTV "jitter" were rather frequent. No significant TTV periodicities were found in the data for any of the stars involved in the analysis, except for the WASP-4 case which is discussed below. The periodogram significance levels were estimated using the approach of Baluev (2008, 2009).

We believe that this indicates a considerable improvement in the statistical quality of the TTV data and/or methods of the statistical analysis, because for the original TTV data from ETD we frequently detected spurious periodicities possibly appearing due to imperfections of the transit fitting algorithm.

5 IMPROVED TRANSIT CURVE PARAMETERS

In addition to the TTV data, we also provide the remaining best fitting parameters of the exoplanetary transit lightcurves. These are the transit parameters that were shared between different lightcurves, and they are given in Table 3. In addition to the previously mentioned transit parameters r, t_d, b, and the limb darkening parameters A and

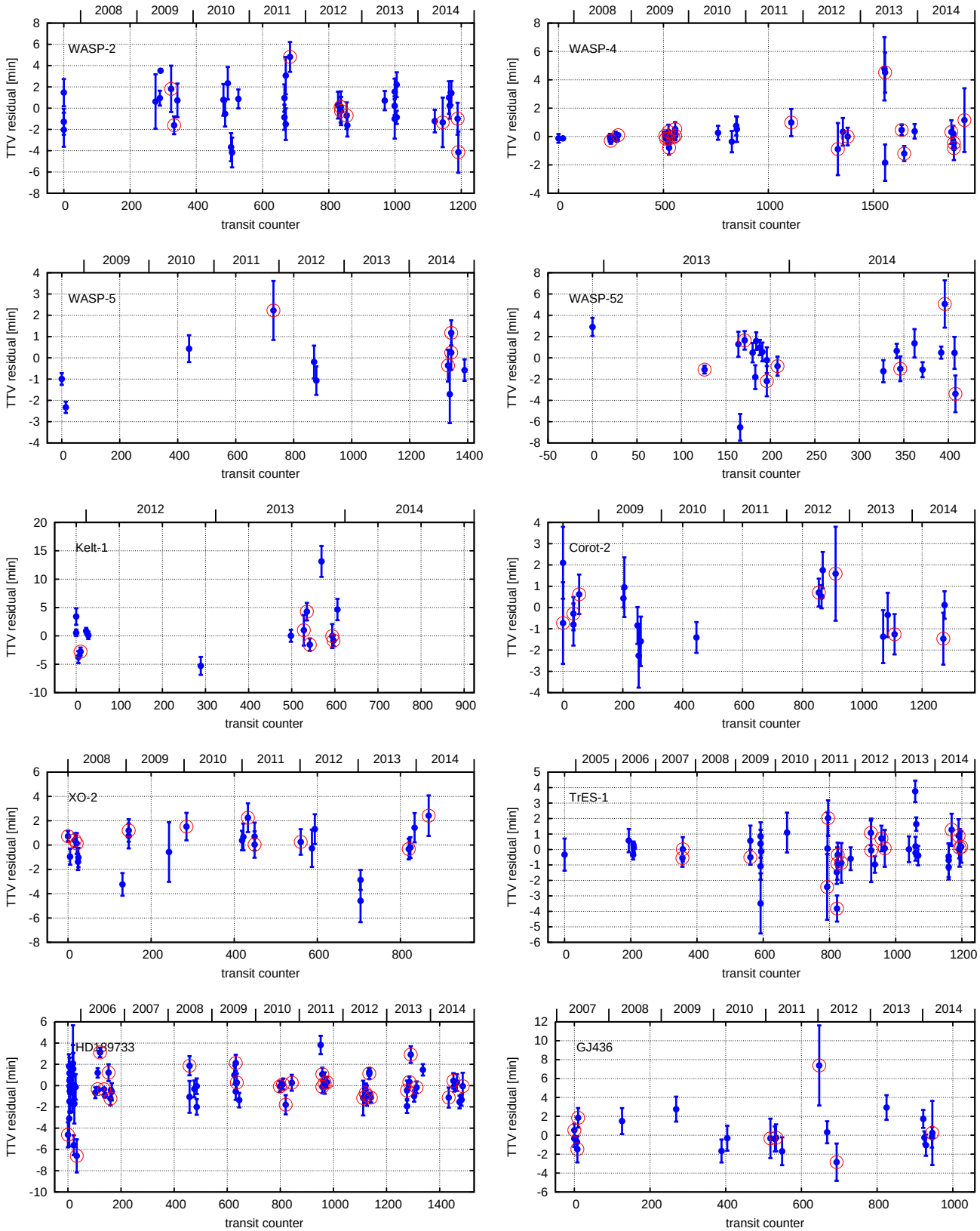


Figure 4. Graphs of the TTV residuals, based on the best fitting transit ephemeris (values of P and $t_c^{\rm ref}$) from Table 3. The transits for which a remarkable red noise was detected in the photometry are labelled with a circle.

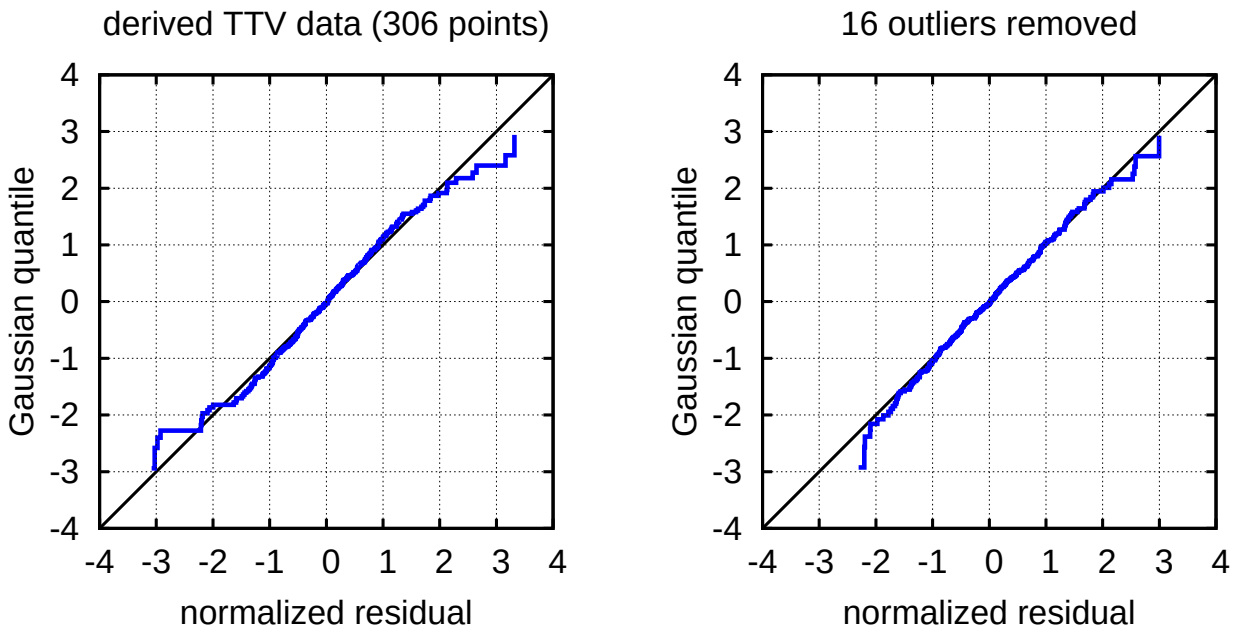


Figure 5. Testing the normality of the TTV data derived in the work. The plot is similar to Fig. 3, but refers to the TTV residuals (relatively to a strictly periodic transit ephemeris) rather than to the photometric ones. In the right panel, we removed the Southworth et al. (2009a,b, 2010) data (7 points), as well as a few potential outliers (9 points).

B, this table also contains the following data: number of the transit lightcurves used in the analysis, number of the lightcurves in which a red noise term was robustly detected, the χ^2 (weighted r.m.s.) of the TTV residuals (relatively to the best linear fit of the derived mid-times), and the refined parameters of the transit emphemeris: transiter period P and a reference mid-time $t_c^{\rm ref}$. The last two quantities were obtained by requiring the mid-times to obey a strict linear relation with the transit count and fitting the coefficients of this relation. The value of $t_c^{\rm ref}$ is not unique due to the periodic nature of the transits. We chose such a fictitious "reference transit", for which the uncertainty of t_c would be minimum. We say this reference transit is fictitious because it should not necessary be actually observed in the survey. This condition simultaneously implies that the correlation between the estimated P and $t_c^{\rm ref}$ is zero.

The $\chi^2_{\rm TTV}$ values in Table 3 always exceed unity, so the fit uncertainties might be moderately underestimated. In some cases this higher than expected scatter could be partly explained by small number of transits involved in the analysis, and in some part it might be due to additional unseen planets that may induce complicated TTV signals and are difficult to detect. Another explanations are incomplete reduction of the red noise and the effect of nonlinearity of the transit model. The latter effect can introduce biases both in the estimated parameters as well as in their uncertainty estimations. So far we could not decide which explanation is more likely. Interesting that this excessive TTV scatter persists and is important even in such a robustly fittable case like HD 189733, in which the model nonlinearity should be well suppressed thanks to a large number of the available observations and lightcurves.

Table 2. Explanation of the TTV data file

column	explanation
	primary data
1	integer transit count (number of the transiter's revolutions, restarts from zero for each star)
2, 3	fitted transit mid-time ($\mathrm{BJD_{TDB}}$) and its uncertainty
	auxiliary data (other parameters of the fit)
4	a standardized name of the lightcurve file that includes the date, the target name, and the name of the observer or first author of a paper
5	the reference time T_0 to which the following trend coefficients refer
6	number of the following trend coefficients including the constant, i.e. the trend degree plus one (always 4 in this work)
7, 8	fitted constant level of the magnitude and its uncertainty
9, 10	fitted linear trend coefficient and its uncertainty ($\mathrm{mag{\cdot}day^{-1}}$)
11, 12	fitted quadratic trend coefficient and its uncertainty ($\mathrm{mag{\cdot}day^{-2}}$)
13, 14	fitted cubic trend coefficient and its uncertainty ($\mathrm{mag{\cdot}day^{-3}}$)
15, 16	fitted limb darkening coefficient A and its uncertainty
17, 18	fitted limb darkening coefficient B and its uncertainty
19	an adopted value of a scale parameter σ_{scale} needed to fully characterize the regularized model of the photometric noise, see (Baluev 2015)
20, 21	fitted photometric white jitter $\sigma_{\star,\mathrm{wht}}$ (def. in Baluev (2015)) and its uncertainty
22, 23	fitted photometric red jitter $\sigma_{\star,\mathrm{red}} = \sqrt{p_{\mathrm{red}}}$ and its uncertainty
24, 25	fitted correlation timescale τ of the red jitter (days)
26	r.m.s. of the best-fit residuals for this lightcurve

Table 3. Fitted parameters of exoplanetary transit curves

transiter	total number of transits	Assuming fittable TTV						Fixing TTV residuals at zero[1]		comment
		number of red-noised transits	radii ratio $r = R_{\rm pl}/R_\star$	half-duration $t_d/2$ [days]	impact par. b	$\sqrt{\chi^2_{\rm TTV}}$ [1]	mid-times correl. MAD/MAX	orbital period P [days]	ref. mid-time $t_c^{\rm ref}$ [BJD$_{\rm TDB}-$ -2450000]	
WASP-2 b	38	9	0.1355(31)	0.03701(35)	0.7380(94)	1.38	0.00056/0.0026	2.15222163(42)	5894.07919(15)	
WASP-4 b	43	20	0.15495(32)	0.044898(53)	0.136(28)	1.35	0.00025/0.0039	1.338231624(68)	4966.782814(21)	
WASP-5 b	11	4	0.1136(13)	0.05028(29)	0.446(40)	1.34	0.0070/0.10	1.62842953(52)	6446.98868(17)	
WASP-52 b	22	7	0.1629(44)	0.03858(69)	0.598(32)	2.00	0.0020/0.016	1.7497835(11)	6673.82149(13)	
Kelt-1 b	18	6	0.0783(14)	0.05661(42)	0.998(44)[2]	2.56	0.00092/0.017	1.21749448(80)	6093.13464(19)	See note 2
Corot-2 b	20	7	0.1639(21)	0.04736(36)	1.000(89)[2]	1.17	0.00079/0.015	1.74299673(31)	5628.44758(14)	See note 2
XO-2 b	25	10	0.1036(13)	0.05563(32)	0.996(31)[2]	1.56	0.00056/0.012	2.61585779(43)	5139.16092(13)	See note 2
TrES-1 b	43	17	0.13781(97)	0.05225(18)	0.191(67)	1.54	0.00038/0.0078	3.03006973(18)	5016.969937(70)	
HD189733 b	67	30	0.15728(35)	0.037556(44)	0.6636(18)	2.12	0.00036/0.073	2.21857492(24)	5956.680364(79)	Some of Bakos et al. (2006) data contain many outliers and possibly non-Gaussian noise
GJ436 b	28	8	0.088(10)	0.02102(71)	0.806(31)	1.22	0.00026/0.0019	2.64389846(44)	5280.17568(17)	Most data are of poor quality (large trends), and a significant eccentricity of ~ 0.15 is not taken into account

[1]The orbital periods, the reference mid-times, and the values of $\chi^2_{\rm TTV}$ were obtained after removal of the Southworth et al. (2009a,b, 2010) data, as these data are affected by clock errors.

[2]Impact parameter b is close to zero and is thus a highly nonlinear parameter here. Its estimation is severely nongaussian, and the formal uncertainty σ_b is much larger than b. To handle this pecularity, the values in the column for b are replaced by $a = \sqrt{1-b^2}$ and its uncertainty $\sigma_a = (b/a)\sigma_b$, which are more informative here.

6 RV DATA AND THEIR ANALYSIS

Additionally to the TTV time series based on the photometry, we also derive RV data for some of our stars, based on the spectra stored in the HARPS archive. We use for this goal spectra found in the HARPS and HARPS-N archive, processing them through the advanced HARPS–TERRA pipeline by Anglada-Escudé & Butler (2012). Public HARPS spectra were available for the following targets: WASP-2, 4, 5, HD 189733, GJ 436, CoRoT-2.

Most of these RV data appeared not very accurate, as many of these targets are rather faint. Moreover, it seems that adequate modelling of these data should involve non-trivial treatment of the RV noise. Frequently, these data are combined in short series acquired within a few hours or even shorter. The data within such single-night series should be significantly correlated (e.g. Nelson et al. 2014), and this effect can be easily detected in some of our data. Usually, these short-term runs were clearly intended to catch a shot of the Rossiter-McLaughlinin effect during the planetary transit. On larger time scales (days to weeks), the RV noise may still remain correlated as well, likely due to the stellar activity (see e.g. Baluev 2013b; Robertson et al. 2014), and this type of correlations is different from the one emerging at short time scales.

The full modelling of all these effects is outside of the scope of this paper, which was intended to deal mainly with the photometry and TTV data. However, these RV data may carry a useful information that can be helpful in verifying the results of our TTV analysis. In this work we adopted a simplified "first look" approach to the RV data analysis. First, we replaced the RV series acquired in a single night by their averages. This eliminated the need to model the Rossiter-McLaughlin effect, as well as the RV noise correlations appearing within a single night. Of course, such a procedure likely adds some systematic error to these "cumulative" measurements, but in this work this is a satisfactory precision. Then we passed these data through a periodogram computing tool of the PlanetPack software, taking into account the best fitting contribution from transiting planet (i.e., including it in the null model of the periodogram).

In this analysis, none of the periodograms revealed hints of any additional variations in the data. Some exception is the GJ 436 case, considered below in more details. In this case we have rather large amount of the HARPS data, as well as Keck data from (Butler et al. 2006), and both these datasets demonstrated clear hints of a red noise, similar to the one investigated e.g. by Baluev (2013b). Modelling this red noise using the methods of that work allowed to get rid of any excessive power in the periodogram, again leaving no significant variations.

7 THE WASP-4 CASE

The periodogram of the WASP-4 TTV data is shown in Fig. 6, and it reveales some marginally significant periodicities, corresponding to the TTV amplitudes $\sim 10-20$ sec. However, there is no any stable pattern of the peaks, as the periodograms are severely model-dependent. Depending on which data subset we include in our analysis, we obtain different results. Note that particularly the data by Southworth et al. (2009b) are not very trustable in TTV studies due to the clock failures noticed for this telescope. This is why we also consider in Fig. 6 a reduced TTV time series obtained by removing these data (only 4 points, but having a good statistical accuracy). Also, results of the period analysis depend on various other subtleties, e.g. on the degree of the polynomial trend used in the photometry model. From the other side, although these variations are marginal and model-dependent, we cannot just attribute them to the noise, as we did not observe anything similar in the other stars of this study.

Using the method of Sect. 4, we detected an outlier in the WASP-4 TTV data, owing to one of the Petrucci et al. (2013) lightcurves. This peculiar lightcurve was already noticed by Petrucci et al. (2013) themselves. Interestingly, the height of the periodogram peak at ~ 5.14 d is *increased* after removal of this TTV outlier from the analysis.

The RV data from the HARPS archive did not reveal any significant signal in addition to the primary transiting planet. However, the star is rather faint for HARPS, and the accuracy of these RV data is not so high, while their reliability is not undoubtful. Also, we should not expect a direct connection between the TTV and RV periods, because often TTV is an indirectly induced variation, owing to the planetary dynamical perturbations. Such a variation may appear due to e.g. a mean motion resonance, which is not always can be easily detected in radial velocities (e.g. Anglada-Escude et al. 2009).

Currently we remain uncertain about the nature of these spurious variations that are possibly present in the WASP-4 TTV data. Possibly, the TTV signal might be more complicated than just a sinusoid, and it should be modelled in the framework of the Newtonian N-body fits. In any case, it seems that we should keep tracking this target or maybe even focus an increased attention on it in the future observations.

8 CONCLUSIONS AND DISCUSSION

As the main topic of the manuscript is the TTV exoplanet detection, it is interesting to investigate its efficiency relatively to the more classic methods like the Doppler planet detection. A TTV signal can be induced via two mechanisms: the dynamical perturbation on the transiter's motion and the light arrival time delay due to the finite light speed (the Roemer effect). The dynamical perturbations are difficult to predict in a general case, as they severely depend on many orbital parameters (e.g. they may drastically increase when planet move in a mean-motion resonance). But the Roemer delay can be easily assessed. Let us assume that a distant second planet has the mass of m and orbits the star (with the transiter) on a circular orbit with the radius of a. Such a planet should induce a similar circular motion of the host star on an orbit of the radius $a' \simeq m/M_\star a$, where $M_\star$ is the star mass. This reduces to a sinusoidal variation of the transits time delay with an amplitude of

$$K_{\rm TTV} \simeq \frac{ma}{cM_\star}, \tag{11}$$

where c is the speed of light.

In the same case, the amplitude of the Doppler variation induced on the star is equal to

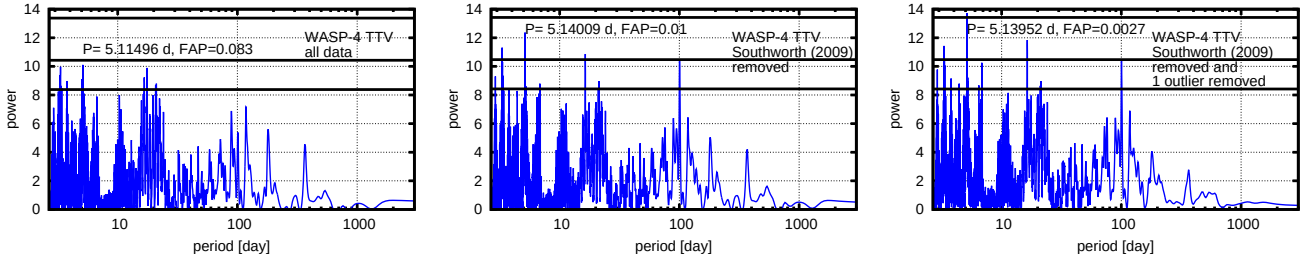


Figure 6. Periodograms of the WASP-4 TTV data, showing a few marginally significant peaks. The plot in the left panel was based on all available transit lightcurves, the middle panel is for a reduced data set with the Southworth et al. (2009b) data removed, and the right panel is for only the ETD data. The thick horizonatal lines label the significance levels of 1σ or FAP ≈ 31.7 per cent, 2σ or FAP ≈ 4.6 per cent, 3σ or FAP ≈ 0.27 per cent. The significance and the period for the tallest peak are printed in each panel. All periodograms involve a quadratic trend of the TTV delay with fittable trend coefficients.

$$K_{\rm RV} \simeq m\sqrt{\frac{G}{aM_\star}}, \tag{12}$$

where G is the gravitational constant. The ratio of these amplitudes now looks like

$$\frac{K_{\rm TTV}}{K_{\rm RV}} \simeq \frac{a^{3/2}}{c\sqrt{GM_\star}} \simeq \frac{P}{2\pi c}, \tag{13}$$

where P is the orbital period of the distant companion, computed according the the third Kepler law. We can see that the relative efficiency of the TTV method, in comparison with the RV one, only depends on the orbital period of the unseen companion.

Contrary to the RV and classic transit surveys, the TTV method is tuned to detect *distant* companions.[1] From this point of view, ground-based observatories should be more useful for TTV planet detection. Spacecrafts rarely operate over a term longer than a few years, while ground-based observations can run on an indefinitely long time base.

The accuracy of the TTV data presented in this work is such that it would allow a robust detection of a signal, if its amplitude is above 1 min. With this TTV threshold, the formula (11) implies that a Jupiter-mass planet orbiting a Solar-mass star could be detected, if its semimajor axis was at least 60 AU, implying an extremely large period of at least ~ 400 yr. This is not a realistic requirement for the observation time. Alternatively, the planet mass should be at least 12 times the Jupiter mass, if we want to detect it at a Jupiter-like orbit with $a = 5.2$ AU. Also, the exoplanet detectability naturally increases for small-mass hosts. Thus, to robustly detect a Jupiter-mass planet, we should either to wait for a long time or to decrease the TTV measurement errors to a level of seconds, roughly by an order of magnitude. Based on these computations, we may say that the TTV detection method is now in its early development stage, comparable to the early era of the Doppler technique (prior or near the 51 Pegasi b detection).

Summarizing, we can conclude that amateur-class TTV observations may occupy two possible niches: (i) detection of long-period massive exoplanets and (ii) detection of exoplanets trapped in mean motion resonances with known transiters (thus generating a more remarkable TTV signal via dynamical effects). However, the TTV detection of long-period Jupiter-like planets might be a feasible task for more advanced ground-based observatories that can achieve the TTV accuracy of a few seconds. Some of the data listed in Table 1 do provide such an accuracy. To enable the detection of Jupiter twins, such observations should be carried out in the monitoring regime, i.e. on a regular basis and over a long term, similar to the modern Doppler surveys. Note that Jupiter analogues may represent a special interest, because such planets would point out exoplanetary systems that have architectures similar to Solar System, in which all giant planets are quite distant from the Sun. The chances to find an Earth twin in such a system might be higher.

At last, we note that the transit fitting algorithm presented here is now implemented in the free PlanetPack package (Baluev 2013a) and should become available with the forthcoming version PlanetPack 2.1 (the current version 2.0 already contains a transit fitting facility, but it was more experimental).

[1] Of course, in any case we must track the variation over at least a single period.

ACKNOWLEDGEMENTS

This work was supported by the Russian Foundation for Basic Research (project No. 14-02-92615 KO_a), by the President of Russia grant for young scientists (No. MK-733.2014.2), and by the programmes of the Presidium of Russian Academy of Sciences P21 and P22.

REFERENCES

Abubekerov M. K., Gostev N. Y., 2013, MNRAS, 432, 2216
Anglada-Escudé G., Butler R. P., 2012, ApJSS, 200, 15
Anglada-Escude G., Lopez-Morales M., Chambers J. E., 2009, ApJL, Submitted, arXiv: 0809.1275
Bakos G. A., et al., 2006, ApJ, 650, 1160
Baluev R. V., 2008, MNRAS, 385, 1279
Baluev R. V., 2009, MNRAS, 393, 969
Baluev R. V., 2011, Celest. Mech. Dyn. Astron., 111, 235
Baluev R. V., 2013a, Astronomy & Computing, 2, 18
Baluev R. V., 2013b, MNRAS, 429, 2052
Baluev R. V., 2015, MNRAS, 446, 1493
Bean J. L., et al., 2008, A&A, 486, 1039
Butler R. P., et al., 2006, ApJ, 646, 505
Carter J. A., Winn J. N., 2009, ApJ, 704, 51

Eastman J., Siverd R., Gaudi B. S., 2010, PASP, 122, 935
Fernandez J. M., Holman M. J., Winn J. N., Torres G., Shporer A., Mazeh T., Esquerdo G. A., Everett M. E., 2009, AJ, 137, 4911
Gillon M., et al., 2009, A&A, 496, 259
Gillon M., et al., 2010, A&A, 511, A3
Knutson H. A., et al., 2014, ApJ, 785, 126
Mayor M., Queloz D., 1995, Nature, 378, 355
Nelson B. E., Ford E. B., Wright J. T., Fischer D. A., von Braun K., Howard A. W., Payne M. J., Dindar S., 2014, MNRAS, 441, 442
Nikolov N., Henning T., Koppenhoefer J., Lendl M., Masiejewski G., Greiner J., 2012, A&A, 539, 159
Petrucci R., Jofré E., Schwartz M., Cúneo V., Martínez C., Gómez M., Buccino A. P., Mauas P. J. D., 2013, ApJ, 779, L23
Pont F., Zucker S., Queloz D., 2006, MNRAS, 373, 231
Pont F., et al., 2007, A&A, 476, 1347
Robertson P., Mahadevan S., Endl M., Roy A., 2014, Science, 25, 440
Sanchis-Ojeda R., Winn J. N., Holman M. J., Carter J. A., Osip D. J., Fuentez C. I., 2011, ApJ, 733, 127
Shporer A., Mazeh T., Pont F., Winn J. N., Holman M. J., Latham D. W., Esquerdo G. A., 2009, ApJ, 694, 1559
Siverd R. J., et al., 2012, ApJ, 761, 123
Southworth J., et al., 2009a, MNRAS, 396, 1023
Southworth J., et al., 2009b, MNRAS, 399, 287
Southworth J., et al., 2010, MNRAS, 408, 1618
Stevenson K. B., et al., 2012, ApJ, 755, 9
Wilson D. M., et al., 2008, ApJ, 675, L113
Winn J. N., et al., 2007a, AJ, 133, 1828
Winn J. N., Holman M., Roussanova A., 2007b, ApJ, 657, 1098
Winn J. N., et al., 2008, ApJ, 683, 1076
Winn J. N., Holman M., Carter J. A., Torres G., Osip D. J., Beatty T., 2009, AJ, 137, 3826

This paper has been typeset from a TEX/ LATEX file prepared by the author.